

# Cosmic Microwave Background Observations: Implications for Hubble's Constant and the Spectral Parameters $n$ and $Q$

Charles H. Lineweaver<sup>1</sup>, Domingos Barbosa<sup>1,2</sup>, Alain Blanchard<sup>1</sup>, and James G. Bartlett<sup>1</sup>

<sup>1</sup> Observatoire astronomique de Strasbourg, U.L.P., 67000 Strasbourg, France.

<sup>2</sup> Centro de Astrofísica da U.P., Rua do Campo Alegre 823, 4150 Porto, Portugal.

Received ; accepted

**Abstract.** Recent cosmic microwave background (CMB) measurements over a large range of angular scales have become sensitive enough to provide interesting constraints on cosmological parameters. In the context of adiabatic perturbations in critical density universes, we use CMB measurements to explore the 4-dimensional parameter space having as free parameters Hubble's constant  $H_o$ , baryonic fraction  $\Omega_b$ , the spectral slope of scalar perturbations  $n$  and the power spectrum quadrupole normalization  $Q$ . We calculate  $\chi^2$  minimization values and likelihood intervals for these parameters. We obtain a low value for Hubble's constant:  $H_o = 30_{-9}^{+13} \text{ km s}^{-1}\text{Mpc}^{-1}$ . The baryonic fraction is not well constrained by the CMB data. The power spectrum slope is  $n = 0.93_{-0.16}^{+0.17}$ . The power spectrum normalization is  $Q = 17.5_{-2.5}^{+3.5} \mu\text{K}$ . These results include estimated uncertainties due to the Saskatoon calibration uncertainty. The error bars on each parameter are for the case where the other 3 parameters have been marginalized. If we condition on  $n = 1$  we obtain the normalization  $Q = 17_{-2}^{+1} \mu\text{K}$ . The permitted regions of the 4-D parameter space are presented in a series of 2-D projections.

Without the CMB data, the combined limits from big bang nucleosynthesis, cluster baryonic fractions and the large scale density fluctuation shape parameter  $\Gamma$  (in the context of cold dark matter  $\Omega_o = 1$ ,  $\lambda_o = 0$  models) yield,  $H_o \approx 35_{-5}^{+6} \text{ km s}^{-1}\text{Mpc}^{-1}$ . For these same cold dark matter models, the CMB data provide a measurement consistent with such a low value for  $H_o$ .

**Key words:** cosmic microwave background — cosmology: observations

---

Send offprint requests to: Charley Lineweaver,  
charley@cdsxb6.u-strasbg.fr

## 1. Introduction

The standard picture of structure formation relies on the gravitational amplification of initially small perturbations in the matter distribution. The origin of these fluctuations is unclear, but a popular assumption is that these fluctuations originate in the very early universe during an inflationary epoch. The most straightforward incarnation of this inflationary scenario predicts that the fluctuations are adiabatic, Gaussian, Harrison-Zeldovich ( $n \approx 1$ ) and that the universe is spatially flat (Kolb & Turner 1990). To avoid violating primordial nucleosynthesis constraints, the universe should be dominated by non-baryonic matter. The cold dark matter (CDM) model has been the preferred model in the inflationary scenario (Peebles 1982, Liddle and Lyth, 1993).

The statistical properties of CMB fluctuations provide an ideal tool for testing CDM models. CMB data offers valuable information not only on the scenario of the origin of cosmic structures, but also on the early physics of the universe and the cosmological parameters that characterize the universe. Using the CMB to determine these parameters is the beginning of a new era in cosmology. This truly cosmological method probes scales much larger and epochs much earlier ( $z > 1000$ ) than more traditional techniques which rely on super-novae, galaxies, galaxy clusters and other low-redshift objects. The CMB probes the entire observable universe.

Acoustic oscillations of the baryon-photon fluid at recombination produce peaks and valleys in the CMB power spectrum at sub-degree angular scales. Measurements of these model-dependent peaks and valleys have the potential to determine many important cosmological parameters to the  $\sim 1\%$  level (Jungman *et al.* 1996). Within the next decade, increasingly accurate sub-degree scale CMB observations from the ground, from balloons and particularly from two new satellites (MAP: Wright *et al.* 1996, COBRAS/SAMBA: Bersanelli *et al.* 1996) will tell us the ultimate fate of the Universe ( $\Omega_o$ ), what the Universe is made of ( $\Omega_b$ ,  $\Omega_{CDM}$ ) and the age and size of the Uni-

verse ( $h \equiv H_o/(100/\text{km s}^{-1}\text{Mpc}^{-1})$ ) with unprecedented precision.

In preparation for the increasingly fruitful harvests of data it is important to determine what the combined CMB data can *already* tell us about the cosmological parameters. In Lineweaver *et al.* (1997), (henceforth “paper 1”), we compared the most recent CMB data to predictions of COBE normalized flat universes with Harrison-Zel’dovich ( $n = 1$ ) power spectra. We used predominantly goodness-of-fit statistics to locate the regions of parameter space preferred by the CMB data. We explored the  $h - \Omega_b$  plane and the  $h - \lambda_o$  plane.

The parameter  $h$  is possibly the most important parameter in cosmology, giving the expansion rate, age and size of the Universe. Current  $h$  measurements are problematic. There may be unknown systematic errors in some or all of the measurements. In such a case it is important to have a different method which, because of its independence, may be free of these unknown systematics. For example, CMB determinations of  $h$  by-pass the local distance ladder. In this paper we focus on the CMB determination of  $h$ .

The parameter  $\Omega_b$  is even less well known than the Hubble constant. Estimates vary by more than a factor of ten, in general roaming within the range  $\sim 2\%$  to  $\sim 20\%$  (White *et al.* 1996).  $\Omega_b$  is important because we would like to know what the universe is made of and how much normal baryonic matter exists in it.

The parameter  $n$  is the primordial power spectrum slope that remains equal to its primordial value at the largest scales (low  $\ell$ ). It is important because it’s measurement is a glimpse at the primordial universe when  $t \ll t(z \approx 1000)$ . Although “backbone” inflation predicts  $n = 1$  (Turner 1996), a larger set of plausible inflationary models is consistent with  $0.7 \lesssim n \lesssim 1.0$ . Model power spectra and particularly the amplitude of the first peak depend strongly on  $n$ . Thus, an important limitation of paper 1 was the restriction to  $n = 1$ . By adding  $n$  as a free parameter we obtain observational limits on  $n$  and quantify the reduced constraining ability of the CMB observations when  $n$  is marginalized.

The power spectrum quadrupole normalization  $Q$  is important because it normalizes all models. Here we treat  $Q$  as a free parameter which we condition on and marginalize over.

In the present paper we have broadened the scope of our exploration to the 4-dimensional parameter space:  $h$ ,  $\Omega_b$ ,  $n$  and  $Q$ . We examine how the constraints on any one of these parameters change as we condition and marginalize over the other parameters. We obtain  $\chi^2$  minimization values and likelihood intervals for  $h$ ,  $\Omega_b$ ,  $n$  and  $Q$ . As in paper 1 we take advantage of the recently available fast Boltzmann code (Seljak and Zaldarriaga 1996) to make a detailed exploration of parameter space. We assume Gaussian adiabatic initial conditions in critical density universes ( $\Omega_o = 1$ ) with no cosmological constant.

We have used the helium fraction  $Y_{He} = 0.24$  and a mean CMB temperture  $T_o = 2.73$ . We ignore the possibility of open universes, early reionization and any gravity wave contribution to the spectra. We do not test topological defect models. We use no hot dark matter.

In Section 2 we describe the data analysis and our treatment of the Saskatoon calibration uncertainty. We present our results and compare them with other work in Section 3. White *et al.* (1996) and de Bernardis *et al.* (1996) using similar data sets have examined high baryonic fraction and early reionization models respectively. Bond and Jaffe (1996) analyzed the combined DMR (Bennett *et al.* 1996), South Pole (Gunderson *et al.* 1995) and Saskatoon (Netterfield *et al.* 1996) data using signal-to-noise eigenmodes. They looked at the parameters  $h$ ,  $n$  and  $\sigma_8$  in a variety of models. In Section 4 we compare and combine our results with other cosmological constraints. In Section 5 we discuss and summarize.

## 2. Method

### 2.1. Calculation

The data used and a two-dimensional  $\chi^2$  calculation are described in paper 1. In this work we have generalized to 4 dimensions and use a likelihood approach to determine the parameter ranges. Thus, for each point in the 4-D parameter space we obtain a value for  $\chi^2(h, \Omega_b, n, Q)$ . At the minimum,  $\chi^2_{min}$ , the parameter values are the best-fit parameters. To obtain error bars on these values, we determine the 4-D surfaces which satisfy  $\chi^2(h, \Omega_b, n, Q) = \chi^2_{min} + x$  where  $x = [1, 4]$ . Under the assumption that the errors on the data points are Gaussian (cf. de Bernardis *et al.* 1996), these ellipsoids can be projected onto any of the axes to get the 68% and 95% confidence intervals for the parameter of that axis (see Press *et al.* 1992 pp 690 for details). To make the figures, we project the ellipsoids onto the two dimensions of our choice and obtain contours which we project onto the axes.

### 2.2. Saskatoon Calibration

We have made estimates of the Saskatoon calibration uncertainty as in paper 1. That is, we did the data analysis three times. Once with all five Saskatoon points at their central values “Sk0”, once with all 5 Saskatoon points increased by 14% “Sk+14”, and once with all 5 Saskatoon points decreased by 14% “Sk-14”.

Netterfield *et al.* (1996) have compared the Saskatoon results to the MSAM results in the north polar region observed by both experiments. They find a best-fit calibration of  $-18\%$ . Preliminary results based on a relative calibration between Jupiter and Cas A at 32 GHz imply that a  $-12\% \pm 3\%$  Saskatoon calibration is appropriate (Leitch *et al.* 1996). In paper 1, we reported that the non-Saskatoon data prefer a  $-24\%$  calibration for the Saskatoon data. Thus a lower calibration may be more appropriate. When

we compare the goodness-of-fits of the minimum  $\chi^2$ , Sk-14 fits are better than the Sk0 fits while Sk+14 fits are poor. Let the probability of obtaining a  $\chi^2_{min}$  value less than that actually obtained be  $P(< \chi)$ . For Sk0, for all cases considered,  $47\% \leq P(< \chi) \leq 55\%$ . For Sk-14, for all cases considered,  $8\% \leq P(< \chi) \leq 15\%$ . For Sk+14,  $P(< \chi)$  are  $> 95\%$ . This is unacceptably large and for the rest of the analysis we ignore the Sk+14 case. We show both the Sk0 and Sk-14 contours in the figures. Since a reasonable case can be made for  $-14\%$  being the preferred calibration, in addition to the best-fit parameters derived from the minimum  $\chi^2$  values for Sk0, we include in Table I the Sk-14 results.

We have normalized the power spectra using the conversion  $C_\ell = Q^2 \frac{4\pi}{5} \frac{C'_\ell}{C'_2}$ , where  $C'_\ell$  is the power spectrum output of the Boltzmann code.

### 3. Results

#### 3.1. Figures and Table

The permitted regions of the 4-D parameter space are presented in a series of 2-D projections which present likelihood contours from a combination of the most recent CMB measurements. There are four groups of figures corresponding to the four planes  $h - \Omega_b$ ,  $h - n$ ,  $h - Q$  and  $n - Q$ : Figures 1 - 6, 7 - 9, 10 - 13 and 14 - 17 respectively.

The thick contours in each figure are from Sk0 while the thin contours are from Sk-14. Areas within the 68% CL contours have been shaded. The thick 'X' marks the Sk0 minimum while the thin 'X' marks the Sk-14 minimum.

The best-fit values and confidence intervals displayed in Figures 1 through 17 are summarized in Table I which thus contains the main results of this work. The values of  $h$ ,  $\Omega_b$ ,  $n$  and  $Q$  at the minimum of the 4-D  $\chi^2$  are given for both Sk0, SK-14. The error bars for Sk0 and Sk-14 come from the projection onto 1-D of the  $\chi^2_{min} + 1$  surface. The separation between the Sk0 and Sk-14 regions is an estimate of the calibration uncertainty. The column labeled "avg" is an average of the Sk0 and Sk-14 results where we have made an effort to correct for the effects of the discretization of the grid underlying the parameter space. The error bars given in this column encompass the 68% contours from both Sk0 and Sk-14 and in this sense include the Saskatoon calibration uncertainty.

#### 3.2. $h - \Omega_b$ Figures

In Figures 1 through 6 the region preferred by big bang nucleosynthesis (BBN) ( $0.010 < \Omega_b h^2 < 0.026$ ) is shaded light grey (c.f. Copi, Schramm & Turner 1995, Tytler & Burles 1996). By comparing Figures 1, 2, 3 and 4 the grey 68% contours can be seen to get bigger as we first condition on and then marginalize over  $n$  and  $Q$ . Conditioning on particular values of the other parameters yields smaller

error bars. The largest uncertainties are obtained when the other 3 parameters are marginalized.

In Figure 1 we have conditioned on  $n = 1$  and  $Q = 18 \mu\text{K}$ . The Sk0 minimum is at ( $h = 0.30$ ,  $\Omega_b = 0.02$ ) while the Sk-14 minimum is at ( $h = 0.37$ ,  $\Omega_b = 0.01$ ).  $\Omega_b$  is very small and there is no overlap of BBN with the 68% CL CMB area.

The contours and notation of Figure 2 are the same as in Figure 1 except that we have let the normalization  $Q$  be a free parameter. That is, for each value of  $h$  and  $\Omega_b$ ,  $Q$  takes on the value (within the discretely sampled range) which minimizes  $\chi^2(h, \Omega_b, Q)$ . Notice that  $h$  stays low, and  $\Omega_b$  is poorly constrained. Only at the 95% CL and only for Sk0 are higher values of  $h$  permitted.

Figure 3 is an example of how, in a 4-D matrix, the discrete values of the parameters can "beat" against each other. That is, increases in one parameter keep the other low until the next discrete value of the other parameter is acceptable. But that new acceptable value is too high and that forces the first one to revert to its previous value. The resulting numerical (but non-physical) oscillations are seen in Figure 3. The effect of discretization can also be seen in the minima reported in Table I. They can be displaced from the true minima by up to half a grid point on both axes (see Figure 7 for an example).

Figure 4 displays the main result for  $h$  of this paper. With both  $n$  and  $Q$  marginalized,  $h$  is confined to a relatively narrow strip around  $h = 0.30$ . There is also a disjoint region of the 4-D ellipsoid which, although it does not contain the minimum, does have  $\chi^2$  values less than  $\chi^2_{min} + 1$ . This same disjoint region is seen in Figures 3, 4, 8, 9 and 13. The high  $h$  disjoint regions in Figures 4, 9 and 13 (where the two non-plotted parameters are free), are consistent in the sense that they yield the same limits on  $h$ . This disjoint region can be characterized by the parameter values  $h \approx 1.00$  ( $h \gtrsim 0.80$ ),  $\Omega_b \approx 0.15^{+0.05}_{-0.06}$ ,  $n \approx 0.77^{+0.11}_{-0.12}$  and  $Q \approx 20^{+2}_{-3} \mu\text{K}$ . The results given in Table I do not include this disjoint region because it is strongly incompatible with the BBN limits. In the  $n - Q$  plane of Figure 17 the region  $n \lesssim 0.8$  and  $Q \gtrsim 20 \mu\text{K}$  (and thus  $h \sim 1.00$ ) is superposed on the low  $h$  region. There is a small notch missing from the Sk0 contour at this juncture.

In Figure 4, the BBN region consistent with large values of  $h$  (lower right of plot) is not favored by the CMB data. Figure 1 suggests that Sk-14 permits higher  $h$  values than the Sk0 analysis, and thus that the plausible reduction of the Saskatoon calibration to -18% or -24% would make  $h \sim 0.60$  compatible with the data. But in the 68% CL regions of Figures 2 and 4, it is Sk0 which allows the highest  $h$  and which is more inclined to produce the narrow strip to high  $h$  at high  $\Omega_b$  (Figure 2).

The most important result we obtain is that with  $\Omega_b$ ,  $n$  and  $Q$  marginalized,  $h \sim 0.30^{+0.13}_{-0.09}$ . Plausible variations in the Saskatoon calibration do not strongly affect our  $h$  result (compare column 2 and 3 of Table 1). In the  $h - \Omega_b$ ,  $h - Q$  and  $h - n$  plots, lowering the Saskatoon

normalization does not raise the acceptable  $h$  value. Thus it does not appear to be the case that a  $-18\%$  or  $-24\%$  Saskatoon calibration will raise the derived  $h$  values. We consider  $h \approx 0.30$  to be a robust CMB result for the  $\Omega_o = 1, \lambda_o = 0$  models tested here.

In Figure 7 there is a strong positive correlation between  $h$  and  $n$ . This can be understood in terms of the peak amplitude  $A_{peak}$  which plays a dominant role in the fitting procedure (see paper 1): as  $h \uparrow$ ,  $A_{peak} \downarrow$  and as  $n \uparrow$ ,  $A_{peak} \uparrow$ , thus if  $h \uparrow$  is accompanied by  $n \uparrow$ ,  $A_{peak}$  can remain unchanged for a certain range of positively correlated  $h$  and  $n$  pairs. This correlation is not seen in Figure 8, where  $\Omega_b$  is a free parameter. The positive correlation between  $h$  and  $Q$  seen in Figure 10 can be explained in the same way. Again, letting  $\Omega_b$  be a free parameter (Figure 11) spoils the correlation.

### 3.3. $\Omega_b$ results

In contrast to  $h$ , our constraints on  $\Omega_b$  are very weak:  $\Omega_b = 0.14^{+0.27}_{-0.14}$ . The 68% confidence interval is larger than the interval explored,  $[0.01, 0.41]$ . As seen in Figure 3, it is the marginalization over  $n$  which opens these contours. White *et al.* (1996) highlight the merits of a high baryonic fraction models ( $\sim 10\% - 15\%$ ). We confirm that the CMB  $\chi^2$  minima fall in this range but the minima are very shallow. SK-14 yields slightly lower values for  $\Omega_b$  than does Sk0. Non-CMB data seems more able to constrain  $\Omega_b$ . See our discussion of Figure 5 in Section 4 where we report  $\Omega_b \approx 0.18 \pm 0.06$ .

### 3.4. $n$ $Q$ results

In Figures 14 through 17 we see that there is a strong correlation between  $n$  and  $Q$ . This has been observed and discussed by many authors (e.g. Smoot *et al.* 1992, Seljak & Bertschinger 1993, Tenorio *et al.* 1996). The increase of the size of the error bars on  $n$  and  $Q$  when the other parameters are marginalized rather than conditioned can be seen by comparing Figures 14, 15, 16 and 17. Our  $n$  and  $Q$  results are  $n = 0.93^{+0.17}_{-0.16}$  and  $Q = 17.5^{+3.5}_{-2.5} \mu\text{K}$  for the case where both  $h$  and  $\Omega_b$  have been marginalized. Conditioning on  $n = 1$ , we get  $Q = 17^{+1}_{-2} \mu\text{K}$ .

The four year COBE-DMR constraints on the amplitude and slope of the power spectrum at large angular scales are  $n_{DMR} = 1.2 \pm 0.3$  and  $Q = 15.3^{+3.8}_{-2.8} \mu\text{K}$ , and conditioning on  $n_{DMR} = 1$ ,  $Q = 18 \pm 1.6 \mu\text{K}$  (Bennett *et al.* 1996). This  $n_{DMR}$  result needs to be corrected due to the mildly model-dependent extended tails of the Doppler peak which reach even into the low  $\ell$  region. After the correction the DMR result becomes  $n \approx 1.05 \pm 0.3$  and  $Q \approx 17.5^{+3.8}_{-2.8} \mu\text{K}$ . Thus the combination of the non-DMR data with the DMR data, agrees well with the DMR-only result and reduces the error bars on  $Q$  slightly. Our  $n$  result is lower than and has error bars approximately half the size of the DMR-only result. In summary, the com-

bination of recent CMB measurements, in the context of critical density universes, marginalized over  $h$  and  $\Omega_b$  gives results consistent with DMR-only results but with smaller error bars.

Using a similar set of data de Bernardis *et al.* (1996) find  $1.0 \leq n \leq 1.26$  (95% CL) for a model with  $\Omega_o = 1$ ,  $h = 0.50$  and  $\Omega_b = 0.05$  without early reionization. For the same model we get the almost identical but slightly lower value  $0.97 \leq n \leq 1.25$  (95% CL). For the same model White *et al.* (1996) get  $0.86 < n < 1.10$  (95% CL) without the CAT data (Scott *et al.* 1996) and letting the Saskatoon calibration be a free parameter. The discrepancy between our results and de Bernardis *et al.*'s results on the one hand, and White *et al.*'s on the other, can be understood from Figure 14, where Sk-14 yields lower values for  $n$ . We know that letting the Saskatoon calibration be a free parameter would amount to setting it equal to  $\sim -20\%$  and thus lower  $n$  values are obtained. Our  $n$  and  $Q$  results when  $h$  and  $\Omega_b$  are marginalized are only weakly dependent on the Saskatoon calibration (compare columns 2 and 3 of Table 1).

## 4. Other Constraints

Other cosmological measurements put independent constraints on parameter space (Bartlett *et al.* 1995):

- Big bang nucleosynthetic results are  $\Omega_b h^2 \approx 0.015^{+0.011}_{-0.05}$  where the errors are dominated by systematics (Copi, Schramm & Turner (1995), Kernan & Krauss 1995, Tytler & Burles 1996). We have adopted the range  $0.010 < \Omega_b h^2 < 0.026$  which encompasses most published results. These limits are plotted in Figures 1 - 6. The regions of the  $h - \Omega_b$  plane acceptable to both the BBN and CMB have low values of  $h$ . The BBN constraints do not depend on our  $\Omega_o = 1$  assumption.

- Cluster baryonic fraction. There are constraints on  $h$  and  $\Omega_b$  from galaxy cluster X-ray data. White *et al.* (1993) generalize a study of the well-studied Coma cluster and obtain  $\Omega_b h^{3/2} = 0.07 \pm 0.03$  for  $\Omega_o = 1$  which is inconsistent with BBN if  $\Omega_b \sim 0.05$ . This has led some to believe that  $\Omega_o < 1$ . However for  $\Omega_b \gtrsim 0.15$ ,  $\Omega_o = 1$  models allow consistency between the CMB, nucleosynthetic and cluster data for low values of  $h$ .

- Large scale density fluctuation shape parameter  $\Gamma$ . Observational limits are  $0.20 \lesssim \Gamma \lesssim 0.30$  (Peacock & Dodds 1994). There is some variation in the literature for the  $\Gamma$  fitting formula (see Sugiyama 1995, Viana & Liddle *et al.* 1996, Bond & Jaffe 1996) but the results are similar. Here we adopt  $\Gamma = \Omega_o h \exp[-\Omega_b - \frac{\Omega_b}{\Omega_o}]$  (Viana & Liddle *et al.* 1996) which is conservative in the sense that for the same given limits on  $\Gamma$  the corresponding  $h$  value is the highest.

- The amplitude of matter fluctuations on small scales ( $\sim 10 h^{-1} \text{ Mpc}$ ) measured by  $\sigma_8$ . Robust estimates independent of  $h$  and  $\Omega_b$  are given by X-ray clusters and

lead to  $\sigma_8 = 0.67 \pm 0.05$  (Oukbir, Blanchard and Bartlett 1996).

- Age of oldest stars. The universe should be older than the oldest stars in our galaxy. There is still some controversy about the stellar ages (see Jimenez 1996, Sarajedmi *et al.* 1995, Chaboyer 1996). Among the various results in the literature, we adopt an age interval that is relatively large so as not to overconstrain the models. Bolte & Hogan (1995) report  $13.7 < t_* < 17.9$  Gyr. For the  $\Omega_o = 1, \lambda_o = 0$  models we are considering here, these age limits can be converted directly into limits on Hubble's constant:  $h < 6.52 \text{ Gyr}/t_*$ , yielding  $0.48 > h > 0.36$  (with the central value 15.8 Gyr corresponding to  $h = 0.41$ ).

#### 4.1. Combined Constraints

Bands illustrating the constraints from BBN, cluster baryonic fraction,  $\Gamma$ , and stellar ages (as described above) are plotted in Figures 5 and 6. To visualize more quantitatively the combination of these constraints, for each constraint, we assume a two-tailed Gaussian distribution around the central values. This allows the flexibility to account for asymmetric error bars. We then calculate a joint likelihood,

$$\mathcal{L}(h, \Omega_b) = \mathcal{L}_{BBN} * \mathcal{L}_{clus} * \mathcal{L}_\Gamma * \mathcal{L}_{CMB}, \quad (1)$$

where,

$$\mathcal{L}_{BBN}(h, \Omega_b) \propto \exp \left[ -\frac{(\Omega_b h^2 - 0.015)^2}{2 \sigma_{BBN}^2} \right] \quad (2)$$

$$\mathcal{L}_{clus}(h, \Omega_b) \propto \exp \left[ -\frac{(\Omega_b h^{3/2} - 0.07)^2}{2 \sigma_{clus}^2} \right] \quad (3)$$

$$\mathcal{L}_\Gamma(h, \Omega_b) \propto \exp \left[ -\frac{(\Gamma(h, \Omega_b) - 0.25)^2}{2 \sigma_\Gamma^2} \right] \quad (4)$$

$$\mathcal{L}_{CMB}(h, \Omega_b) \propto \exp \left[ -\frac{\chi^2(h, \Omega_b)}{2} \right]. \quad (5)$$

The upper and lower limits of the four constraints determine the  $\sigma$ 's for the two tailed Gaussians. For example  $\sigma_{BBN,up} = (0.026 - 0.015)$  and  $\sigma_{BBN,down} = (0.015 - 0.010)$ .  $\mathcal{L}_{CMB}$  is shown in Figure 4.  $\mathcal{L}_{BBN} * \mathcal{L}_{clus} * \mathcal{L}_\Gamma$  is shown in Figure 5. The joint likelihood of all 4 terms ( $\mathcal{L}_{CMB} * \mathcal{L}_{BBN} * \mathcal{L}_{clus} * \mathcal{L}_\Gamma$ ) is shown in Figure 6. The contour levels in Figure 5 and 6 are  $\mathcal{L}(h, \Omega_b)/\mathcal{L}_{max} = \exp(-\frac{1}{2}[1, 4])$ . The combined non-CMB constraints from BBN, cluster baryonic fraction and  $\Gamma$  shown in Figure 5 yield  $h \sim 0.35^{+0.06}_{-0.05}$  and  $\Omega_b = 0.19^{+0.06}_{-0.07}$  (for  $\Omega_o = 1 | \lambda_o = 0$ ).

Comparing Figures 4 and 5 we see that the combination of three independent cosmological measurements indicate the same low value as the CMB data in the context of the CDM models considered here; in this sense our low CMB values for  $h$  are not surprising (Bartlett *et al.* 1995). Including the CMB to produce an approximate joint likelihood (Figure 6) yields very similar results:  $h \sim 0.33^{+0.06}_{-0.05}$  and  $\Omega_b = 0.20^{+0.07}_{-0.06}$ .

#### 5. Discussion and Summary

Liddle *et al.* (1996) studied critical density CDM models. Based on the COBE normalization, peculiar velocity flows, the galaxy correlation function, abundances of galaxy clusters, quasars and damped Lyman alpha systems, they found that  $h < 0.50$  and  $n < 1$  is preferred. Adams *et al.* (1996) come to similar conclusions. Results from the distribution of objects at  $z \sim 0$  are in very good agreement with the results found here which are based on the properties of the universe at  $z \approx 1100$  in the context of critical density models. We propose that the best critical density CDM model is  $h \approx 0.30$ ,  $\Omega_b \sim 0.15$ ,  $n \approx 0.95$  and  $Q \approx 17.5 \mu\text{K}$ .

The amplitude of small scale matter fluctuations provides an additional consistency check on this model. The corresponding amplitude is  $\sigma_8 \approx 0.7$  which is in agreement with the independent value of  $\sigma_8$  inferred from X-ray cluster data.

Bartlett *et al.* (1995) listed the advantages of a low  $h$  in critical density universes. Notable among them is the age crisis. Recent  $h$  measurements point to values in the interval  $0.60 < h < 0.80$ . In a critical density universe  $h = 0.70$  implies an age of 9.3 Gyr, younger than the estimated age of many globular clusters.  $h = 0.30$  yields an age for the universe of 21.7 Gyr comfortably in accord with globular cluster ages. Our CMB results can now be added to the list of observational evidence that indicates that if  $\Omega_o = 1$ , then  $h \sim 0.30$  is to be favored.

CMB measurements have become sensitive enough to constrain cosmological parameters. In the context of adiabatic perturbations in critical density universes, we have explored the 4-dimensional parameter space of  $h$ ,  $\Omega_b$ ,  $n$  and  $Q$ . We have presented the permitted regions of the 4-D parameter space in a series of 2-D projections. We obtain a low value for Hubble's constant:  $H_o = 30^{+13}_{-9}$ . We obtain strong constraints on the slope and normalization of the power spectrum:  $n = 0.93^{+0.17}_{-0.16}$  and  $Q = 17.5^{+3.5}_{-2.5} \mu\text{K}$ . The CMB data constrains  $\Omega_b$  only weakly:  $\Omega_b = 0.14^{+0.27}_{-0.14}$ .

These results include estimated uncertainties due to the Saskatoon calibration uncertainty. The error bars on each parameter are for the case where the other 3 parameters have been marginalized. When we condition on  $n = 1$  we obtain the normalization  $Q = 17^{+1}_{-2} \mu\text{K}$ .

Without the CMB data, the combined limits from BBN, cluster baryonic fraction and the shape parameter  $\Gamma$  (in the context of  $\Omega_o = 1, \lambda_o = 0$  models) yield  $H_o \approx 35^{+6}_{-5}$ . Within the context of critical density universes, our low  $H_o$  results from the CMB are consistent with these earlier independent constraints.

Our CMB-derived constraints on  $h$ ,  $n$  and  $Q$  are fairly strong and large regions of parameter space are excluded. CMB constraints are independent of other cosmological tests of these parameters and are thus particularly important. The fact that there are regions of parameter space

where CMB results overlap with other methods is an important consistency check.

The results we have presented here are valid under the assumption of Gaussian adiabatic initial conditions in a critical density universe ( $\Omega_o = 1$ ) with no cosmological constant. The rapidly increasing quality and quantity of data along with fast Boltzmann code kindly provided by Uros Seljak and Matias Zaldarriaga has made this work possible. We thank Martin White, Douglas Scott and the Max group for help assembling the required experimental window functions. We thank Luis Tenorio for statistics counseling. C.H.L. acknowledges support from the French Ministère des Affaires Etrangères and NSF/NATO post-doctoral fellowship 9552722. D.B. is supported by the Praxis XXI CIENCIA-BD/2790/93 grant attributed by JNICT, Portugal.

- Turner, M. 1996, (Strasbourg CMB school)
- Tytler, D. & Burles, S. 1996, Atami Proceedings
- Viana, P.T.P & Liddle, A.R. 1996, MNRAS, 281, 323
- White, S. D.M. 1993, Nature, 366, 429
- White, M. Viana, P.T.P, Liddle, A.R., Scott, D. MNRAS, 283, 107
- Wright, E.L., Hinshaw, G. & Bennett, C.L. 1996, Ap.J., 458, L53

## References

- Adams, J.A., Ross, G.G., Sarkar, S. 1996, Phys. Rev. B in press (hep-ph/9608336)
- Bartlett, J. Blanchard, A., Silk, J., Turner, M., 1995, Science, 267, 980
- Bennett, C. L., et al. 1996, Ap.J., 464, L1
- Bersanelli, M. et al. February, 1996, COBRAS/SAMBA phase A study, ESA Report(D/SCI(96)3)
- Bolte, M. & Hogan, C. 1995, Nature, 376, 399
- Bond, J. R. et al. *Astrophys. Lett. and Comm.*, 32, 1-6, p53, 1995
- Bond, J. R. & Jaffe, A. H. Moriond proceedings, astro-ph 9610091
- Chaboyer, B. Ap.J. 444, L9
- Copi, C.J., Schram, D. N. & Turner, M.S., Science, 267, 192 (1995)
- de Bernardis, P. 1996, Ap.J. submitted, astro-ph/9609154
- Dodelson, S., Gates, E.I. & Turner M.S. 1996, Science, 274, 69
- Gunderson, J.O. Ap.J., 443, L57
- Jimenez, et al. 1996, MNRAS, 1995,
- Jungmann, et al. 1996, Phys. Rev. D. 54, 1332
- Kolb, E.W. & Turner, M.S. 1990, "The Early Universe", Addison-Wesley:Redwood City
- Leitch, E. et al. 1997, in preparation
- Liddle A. R. & Lyth D. 1993, Phys. Rep. 231, 1
- Liddle A. R. et al. 1996, MNRAS, 281, 531
- Lineweaver, C.H., Barbosa, D., Blanchard, A. & Bartlett, J.G. 1997, A&A in press, astro-ph/9610133
- Netterfield, C. B. et al. 1995, ApJ, 445, L69
- Oukbir, J., Blanchard, A. & Bartlett, J.G. 1997, A&A in press astro-ph/9611089
- Peacock, J.A. & Dodds, S.J. MNRAS, 267, 1020, 1994
- Peebles, P.J.E., 1982, Ap.J., 263, L1
- Sarajedimi, Ap.J., 450, 712
- Scott, P.F.S. et al. , 1996, Ap.J., 461, L1
- Seljak, U. & Bertschinger, E. 1993, Ap.J., 417, L9
- Seljak, U. & Zaldarriaga, M., 1997, Ap.J.in press, astro-ph/9603033
- Smoot, G.F. et al. 1992, Ap.J. 396, L1
- Sugiyama, N. 1995, Ap.J. Sup. Ser., 100, 281
- Tenorio,L., Lineweaver,C.H., Smoot, G.F. 1997, J. Royal Statistical Society, series D, (The Statistician) submitted

Table I: Parameter Results

	Results		Conditions				
	Sk0 <sup>a</sup>	Sk-14 <sup>a</sup>	avg <sup>b</sup>	h	$\Omega_b(\%)$	n	$Q(\mu\text{K})$
$H_o =$	$30_{-4}^{+4}$	$37_{-4}^{+5}$	$34_{-8}^{+8}$	—	free <sup>c</sup>	1	18
	$30_{-6}^{+12}$	$35_{-7}^{+3}$	$33_{-9}^{+9}$	—	free	1	free
	$30_{-9}^{+14}$	$30_{-9}^{+8}$	$30_{-9}^{+14}$	—	free <sup>d</sup>	free	18
	$30_{-8}^{+5}$	$25_{-4}^{+13}$	$29_{-8}^{+9}$	—	5	free	18
	$30_{-6}^{+13}$	$35_{-8}^{+8}$	$32_{-8}^{+11}$	—	5	1	free
	$30_{-7}^{+6}$	$30_{-7}^{+8}$	$30_{-7}^{+8}$	—	5	free	free
	$30_{-7}^{+10}$	$30_{-9}^{+13}$	$30_{-9}^{+13}$	—	free <sup>d</sup>	free	free
$\Omega_b(\%) =$	$2_{-1}^{+3}$	$1_{-1}^{+2}$	$2_{-2}^{+3}$	free	—	1	18
	$5_{-3}^{+17}$	$2_{-2}^{+5}$	$3_{-3}^{+19}$	free	—	1	free
	$25_{-9}^{+15}$	$10_{-10}^{+27}$	$17_{-17}^{>+23}$	free	—	free	18
	$25_{-0.25}^{+>15}$	$3.5_{-3.5}^{+>38}$	$14_{-14}^{+>27}$	free <sup>d</sup>	—	free	free
$n =$	$0.97_{-0.04}^{+0.03}$	$0.91_{-0.03}^{+0.06}$	$0.95_{-0.07}^{+0.05}$	free	5	—	18
	$0.91_{-0.07}^{+0.10}$	$0.91_{-0.09}^{+0.10}$	$0.91_{-0.09}^{+0.10}$	free	free	—	18
	$1.15_{-0.07}^{+0.04}$	$1.03_{-0.03}^{+0.11}$	$1.10_{-0.10}^{+0.09}$	50	5	—	free
	$1.03_{-0.11}^{+0.05}$	$0.97_{-0.12}^{+0.05}$	$0.98_{-0.13}^{+0.10}$	free	5	—	free
	$0.91_{-0.06}^{+0.17}$	$0.97_{-0.21}^{+0.05}$	$0.94_{-0.18}^{+0.14}$	30	free	—	free
	$0.91_{-0.10}^{+0.19}$	$0.97_{-0.20}^{+0.13}$	$0.93_{-0.16}^{+0.17}$	free <sup>d</sup>	free	—	free
$Q(\mu\text{K}) =$	$17_{-1}^{+1}$	$17_{-2}^{+1}$	$16.5_{-1.5}^{+1.5}$	free	5	1	—
	$17_{-2}^{+1}$	$17_{-1}^{+1}$	$17_{-2}^{+1}$	free	free	1	—
	$15_{-1}^{+2}$	$17_{-3}^{+1}$	$16_{-2}^{+2}$	50	5	free	—
	$16_{-1}^{+3}$	$17_{-1}^{+3}$	$16.5_{-1.5}^{+3.5}$	free	5	free	—
	$18_{-2.5}^{+3}$	$17_{-1}^{+4}$	$17.5_{-2}^{+3.5}$	30	free	free	—
	$18_{-2}^{+2}$	$17_{-2}^{+4}$	$17.5_{-2.5}^{+3.5}$	free <sup>d</sup>	free	free	—

<sup>a</sup> parameter values at the  $\chi^2$  minimum for the cases Sk0 and Sk-14 (see Section 2.2). The error bars of Sk0 and Sk-14 reflect the size of the 68% CL contours in the figures and thus do not include the calibration uncertainty.

<sup>b</sup> “avg” values are the average of the Sk0 and Sk-14 except that they also include our effort to compensate for the effects of the discrete grid underlying the parameter space. The error bars given encompass the 68% CL contours from both Sk0 and Sk-14 and in this sense include the Saskatoon calibration uncertainty.

<sup>c</sup> “free” means that the parameters were free to take on any values within the discretely sampled range which minimized the value of  $\chi^2$ . The discretization of the sampled range is partially visible in Figure 3. As a result of the discretization, the reported value  $H_o = 30$  should be taken to mean,  $27.5 \leq H_o \leq 32.5$ . The underlying matrix of model points is described by  $0.15 \leq h \leq 1.00$ , step size: 0.05,  $0.01 \leq \Omega_b \leq 0.4$ , step size: 0.012,  $0.5 \leq n \leq 1.5$ , step size: 0.06,  $10 \leq Q \leq 30$ , step size: 1. Thus we have tested over 200,000 ( $18 \times 34 \times 18 \times 20$ ) models.

<sup>d</sup> There is a disjoint region of the 4-D ellipsoid which is not included in these error bars. See Section 3.2 for discussion.

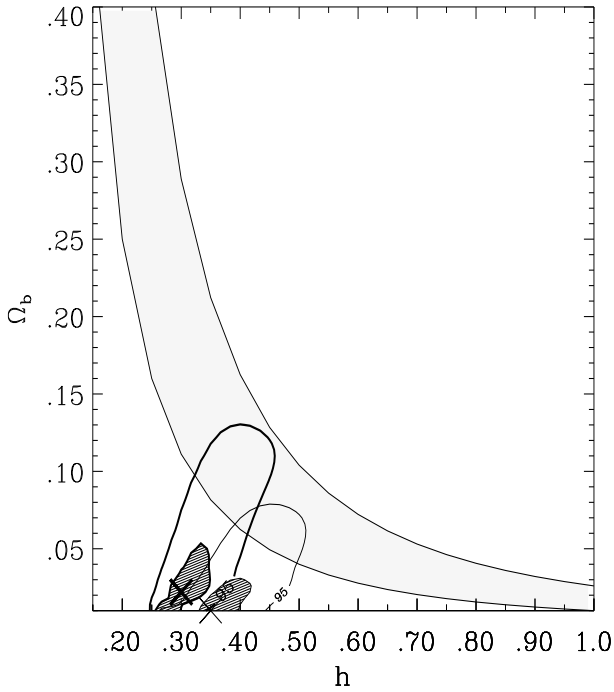


**Fig. 1.** Likelihood contours in the  $h - \Omega_b$  plane from a combination of the most recent CMB measurements. The thick contours are from Sk0 while the thin contours are from Sk-14 (see Section 2.2). The contours are at levels  $\chi^2_{min} + x$  where  $x = [1, 4]$ . When projected onto either of the axes these regions give the approximate size of the 68% and 95% confidence intervals respectively. Areas within the 68% contours have been shaded. We have conditioned on  $n = 1$  and  $Q = 18 \mu\text{K}$ . The thick 'X' marks the Sk0 minimum ( $h \approx 0.30, \Omega_b \approx 0.02$ ) while the thin 'X' marks the Sk-14 minimum ( $h \approx 0.35, \Omega_b \approx 0.01$ ). Big bang nucleosynthesis predictions favor the band in grey defined by  $0.010 < \Omega_b h^2 < 0.026$ . It appears that a lower Saskatoon calibration implies a higher  $h$ , but see the following figures.

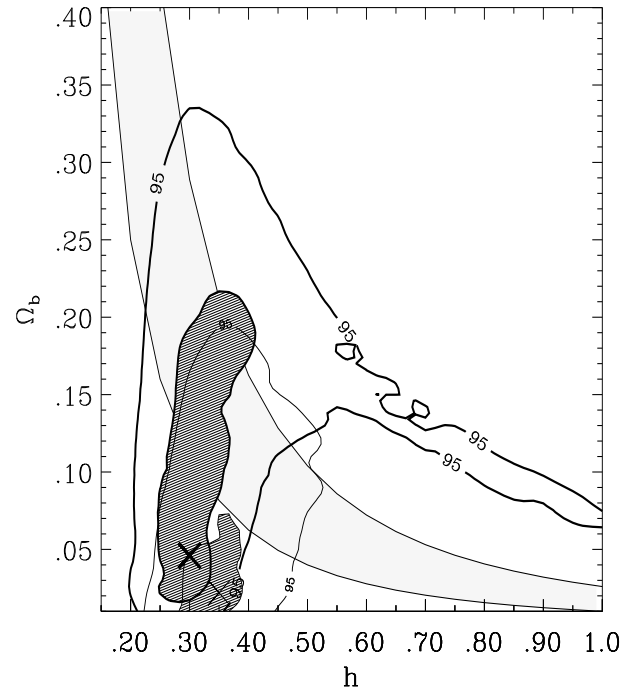


**Fig. 2.** Contours and notation as in previous figure except here we have conditioned on  $n = 1$  and  $Q$  has been left as a free parameter which for a given  $h$  and  $\Omega_b$ , takes on the value that minimizes the value of  $\chi^2$  at that point. When compared with the previous figure, allowing  $Q < 18 \mu\text{K}$  here shifts the Sk0 68% CL region up and to the left. Thus the grey regions from the previous figure are not necessarily subsumed in the grey regions here.

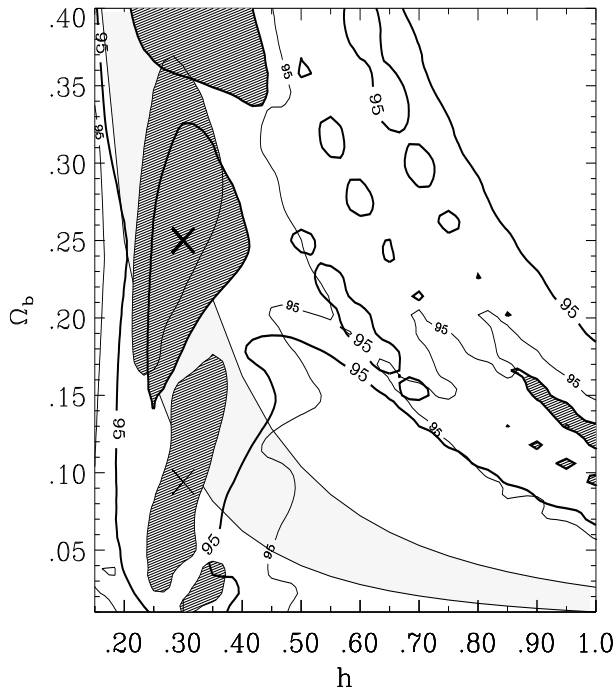


**Fig. 3.** Contours as in previous figure except here we have conditioned on  $Q = 18 \mu\text{K}$  and marginalized on  $n$ . Apparently, due to the discretization of the matrix,  $n$ ,  $h$  and  $\Omega_b$  are “beating” against each other (see Section 3.2). The underlying matrix of model points is described by  $0.15 \leq h \leq 1.00$ , step size: 0.05,  $0.01 \leq \Omega_b \leq 0.4$ , step size: 0.012,  $0.5 \leq n \leq 1.5$ , step size: 0.06,  $10 \leq Q \leq 30$ , step size: 1.

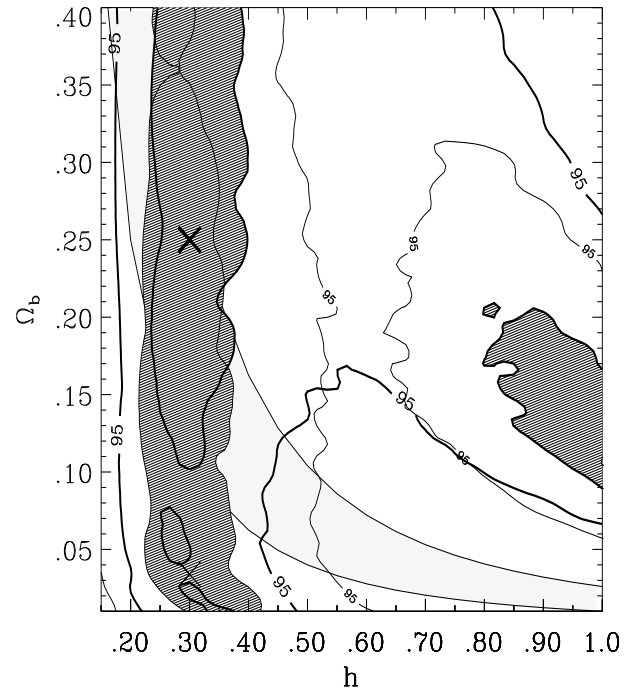


**Fig. 4.** Same as previous figure except we have marginalized over both  $n$  and  $Q$ .  $h$  stays low. Note that it is not true that a lower Saskatoon calibration permits higher values of  $h$ . The region at high  $h$  disjoint from the minimum is acceptable in the sense that the  $\chi^2$  values from Sk0 (but not from Sk-14) are less than  $\chi^2_{\min} + 1$ . This region has  $n \sim 0.8$  and  $Q \sim 20 \mu\text{K}$  and can be excluded if the BBN prediction is taken seriously. See also Figures 8, 9 and 13.

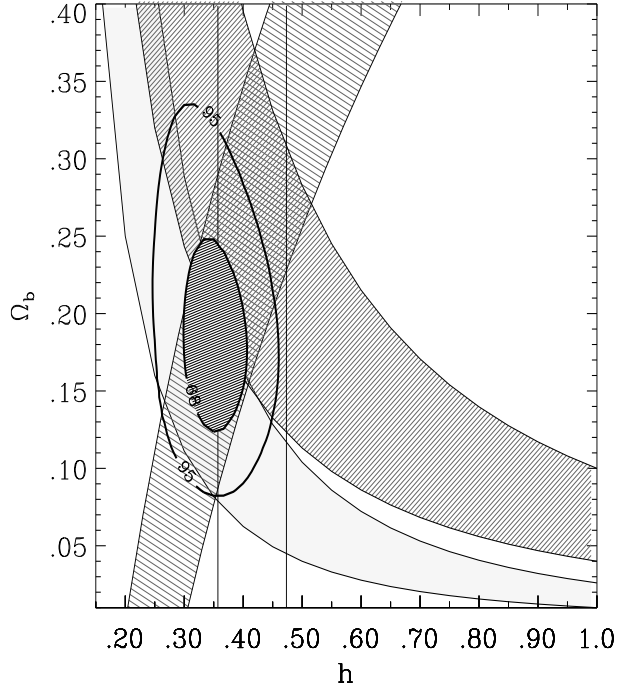


**Fig. 5.** This plot has no CMB information in it. The bands are the constraints from 4 non-CMB measurements: BBN as before, cluster baryonic fraction (White *et al.* (1993), the shape parameter  $\Gamma$  from galaxy and cluster scale density fluctuations (Peacock & Dodds 1994) and the constraint on  $h$  from the age of the oldest stars in globular clusters (Bolte & Hogan 1995)  $13.7 < t_o < 17.9$  which, for  $\Omega_o = 1$ ,  $\lambda_o = 0$  is equivalent to  $48 > H_o > 36$  (region between the vertical lines in figure). To quantify the combination of the BBN, baryonic fraction and  $\Gamma$  constraints we show contours obtained by assuming for each constraint a two-tailed Gaussian probability around the central values (see Section 4). This is thus an approximate joint likelihood of 3 non-CMB constraints. A low  $h$  is preferred. This was pointed out in Bartlett *et al.* (1995). The combination of these three, independent, non-CMB measurements yields  $H_o \sim 35^{+6}_{-5}$  and  $\Omega_b = 0.19^{+0.06}_{-0.07}$ . This is a region of the  $h - \Omega_b$  plane that is very similar to the region preferred by the CMB data (compare Figure 4). Other methods to determine  $h$  find higher values.

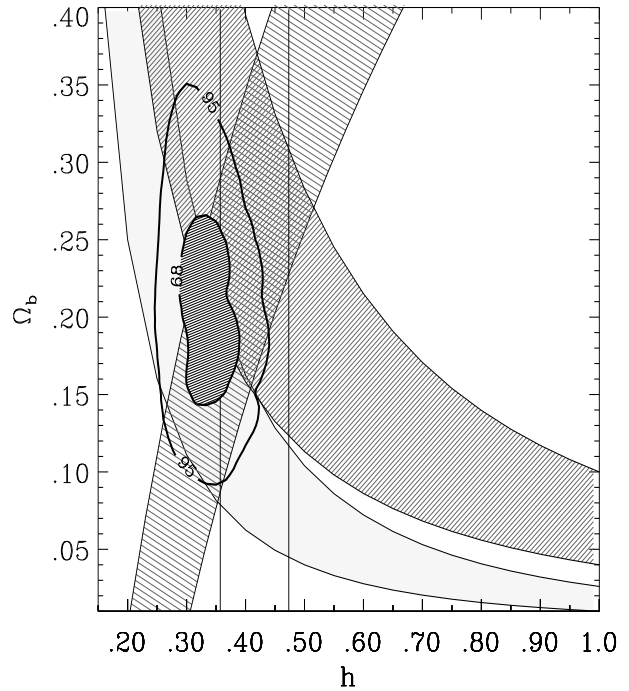


**Fig. 6.** Here we have combined the CMB constraints of Figure 4 (Sk0) with the non-CMB constraints of Figure 5. That is, we have multiplied the approximate joint likelihoods of Figure 5 by the  $\mathcal{L}_{CMB}(h, \Omega_b)|_{Sk0, n=free, Q=free}$  of Figure 4. Result:  $H_o \approx 33^{+6}_{-5}$  and  $\Omega_b \approx 0.20^{+0.07}_{-0.06}$ .

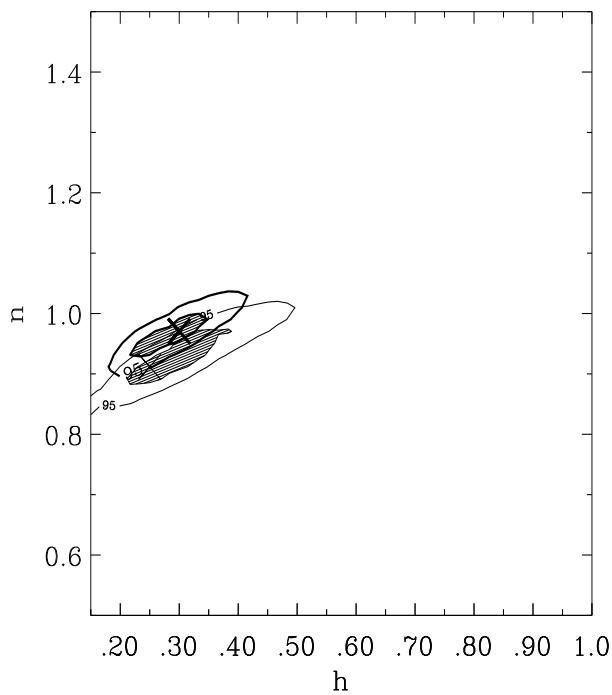


**Fig. 7.** Likelihood contours in the  $h - n$  plane for  $Q = 18 \mu\text{K}$  and  $\Omega_b = 0.05$ . Discretization of the underlying matrix displaces the minima ('X' symbols) slightly from the real minimum by up to half a grid spacing. The positive correlation between  $h$  and  $n$  is discussed in Section 3.2.

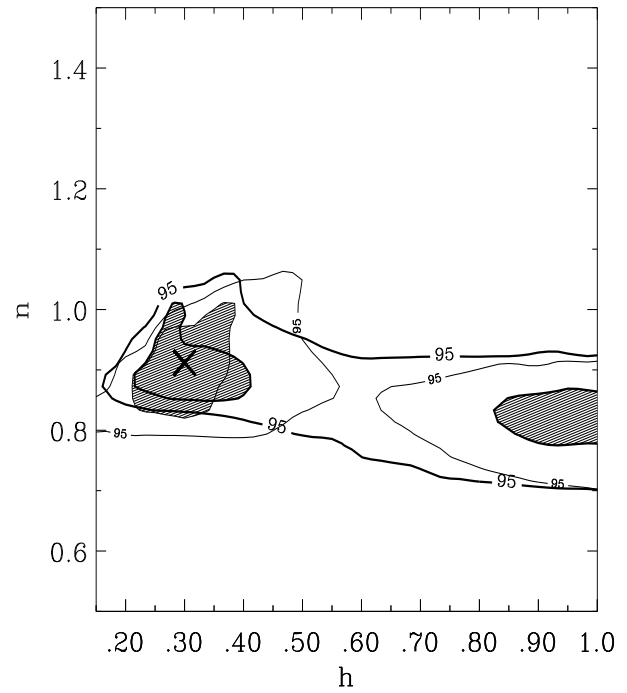


**Fig. 8.** Likelihood contours in the  $h - n$  plane for  $Q = 18 \mu\text{K}$  and  $\Omega_b$  is a free parameter. The Sk-14 minimum is identical with the Sk0 minimum. The acceptable region for  $h \gtrsim 0.75$  has a slightly lower  $n$  than the minimum at low  $h$ . Since  $Q$  is fixed in this plot and  $n$  is correlated with  $Q$ ,  $n$  cannot go down as much as it would like (compare the next figure). Allowing  $\Omega_b \gtrsim 0.10$  opens up this high  $h$  region.

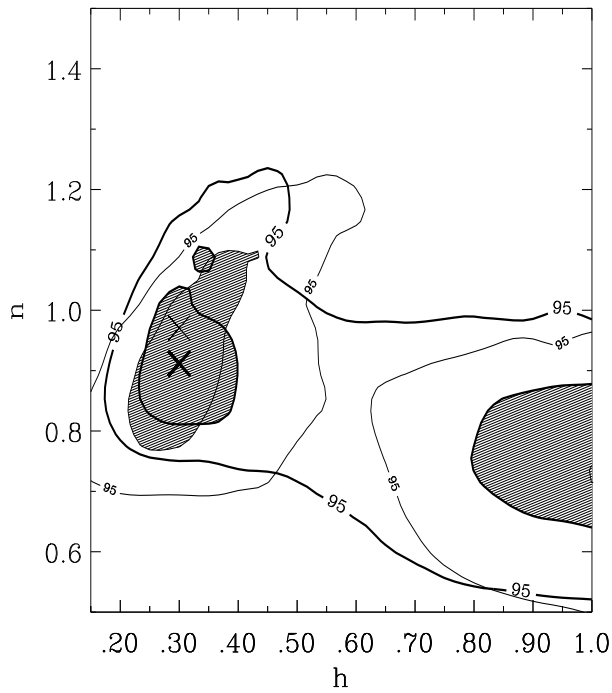


**Fig. 9.** Likelihood contours in the  $h - n$  plane for  $\Omega_b$  free and  $Q$  free. The acceptable region for  $h \gtrsim 0.80$  has  $Q \sim 20 \mu\text{K}$  (see Figure 13).

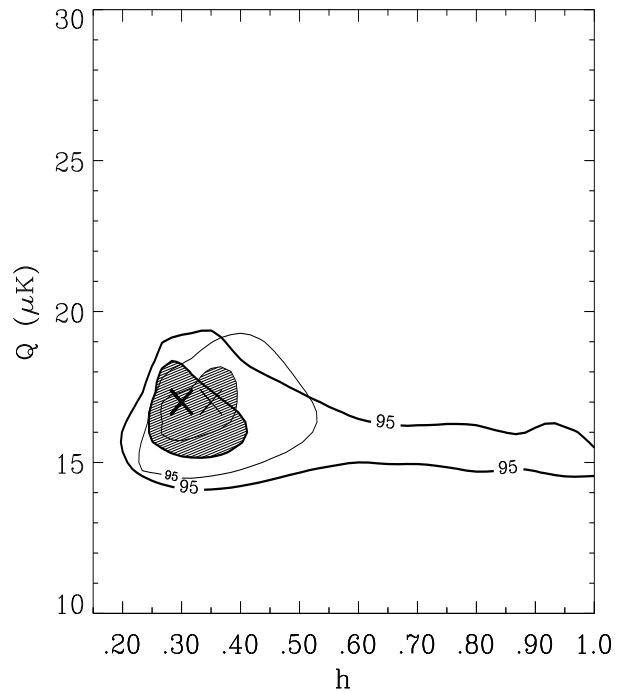


**Fig. 11.** Likelihood contours in the  $h - Q$  plane for  $n = 1$  and  $\Omega_b$  free. Notice that since  $n$  has been fixed at 1, the value of  $Q$  does not rise in the high  $h$  region.

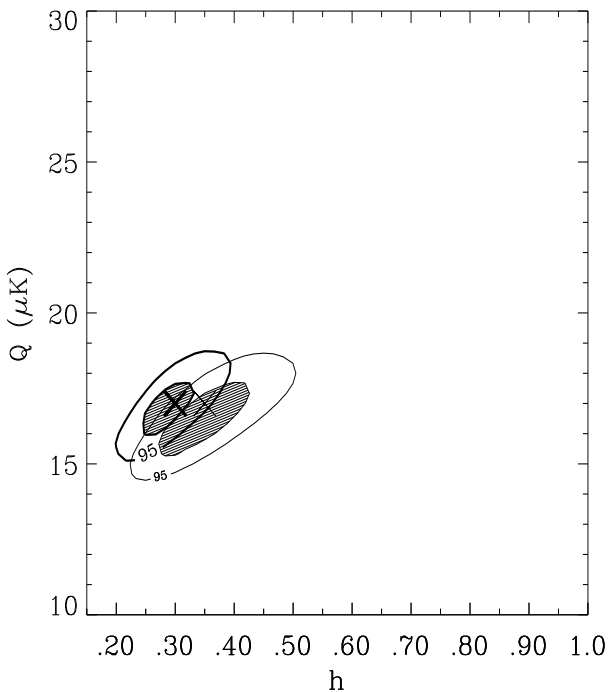


**Fig. 10.** Likelihood contours in the  $h - Q$  plane for  $n = 1$  and  $\Omega_b = 0.05$ .

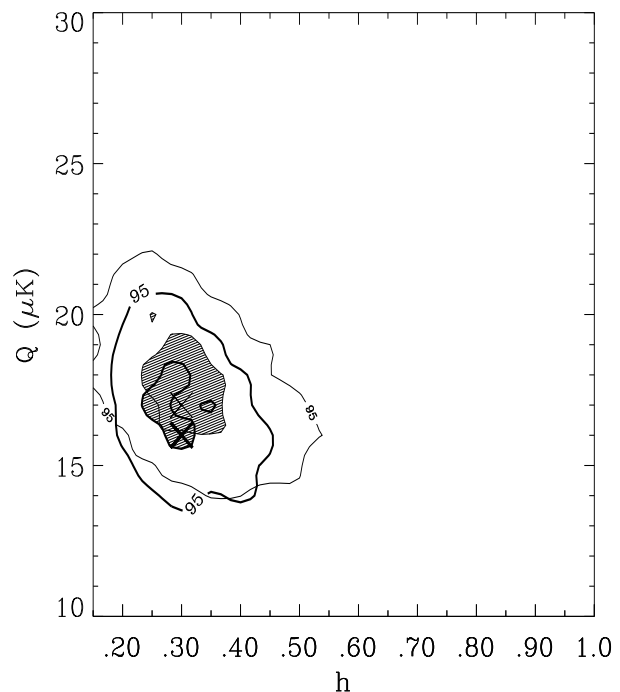


**Fig. 12.** Likelihood contours in the  $h - Q$  plane for  $\Omega_b = 0.05$  and  $n$  free.

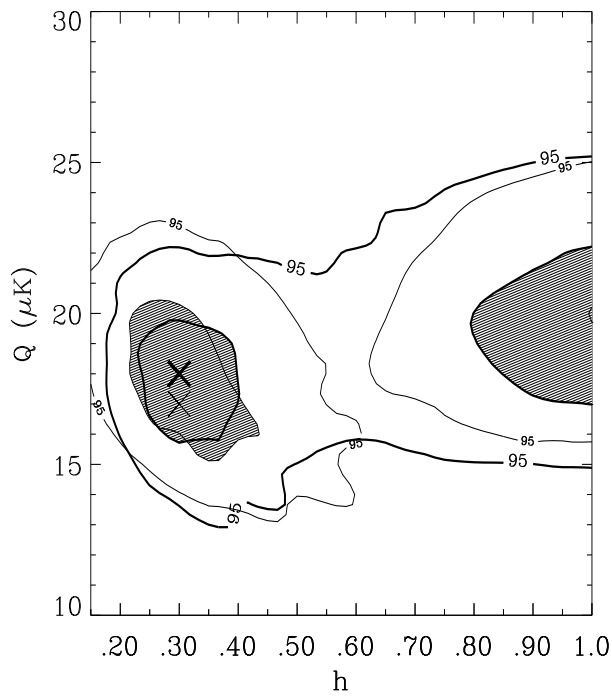


**Fig. 13.** Likelihood contours in the  $h - Q$  plane for  $n$  free and  $\Omega_b$  free. Notice that in the high  $h$  region,  $Q \sim 20 \mu\text{K}$  is preferred.

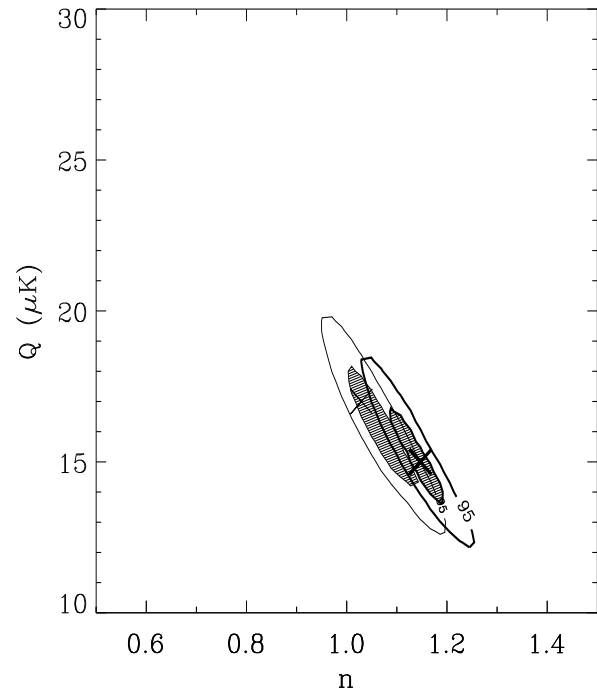


**Fig. 14.** Likelihood contours in the  $n - Q$  plane for  $h = 0.50$  and  $\Omega_b = 0.05$ . This is a model looked at by de Bernardis *et al.* (1996) who obtain similar results. White *et al.* (1996) obtain lower results but for the case of using the Saskatoon calibration as a free parameter which we estimate amounts to using a calibration of  $\sim -20\%$  (see Section 3.4).

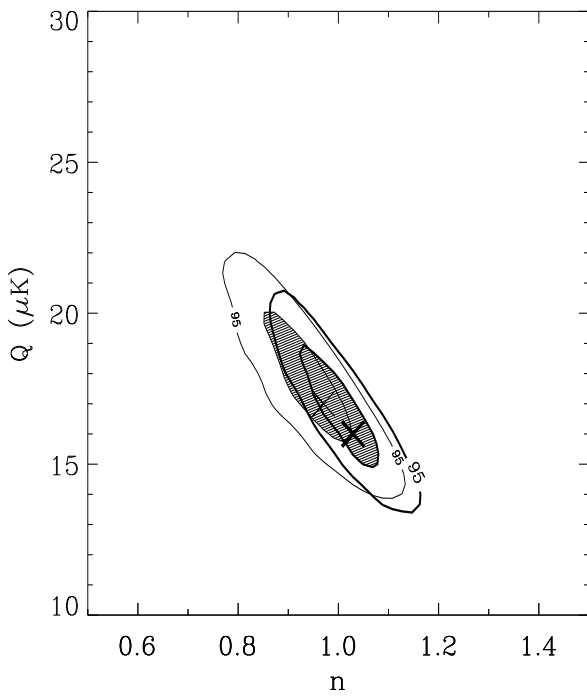


**Fig. 15.** Likelihood contours in the  $n - Q$  plane for  $\Omega_b = 0.05$  and  $h$  free.

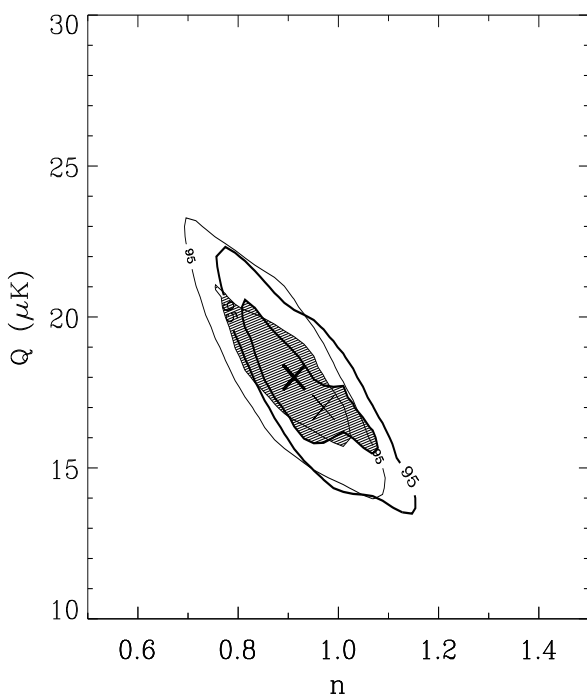


**Fig. 16.** Likelihood contours in the  $n - Q$  plane for  $h = 0.30$  and  $\Omega_b$  free.

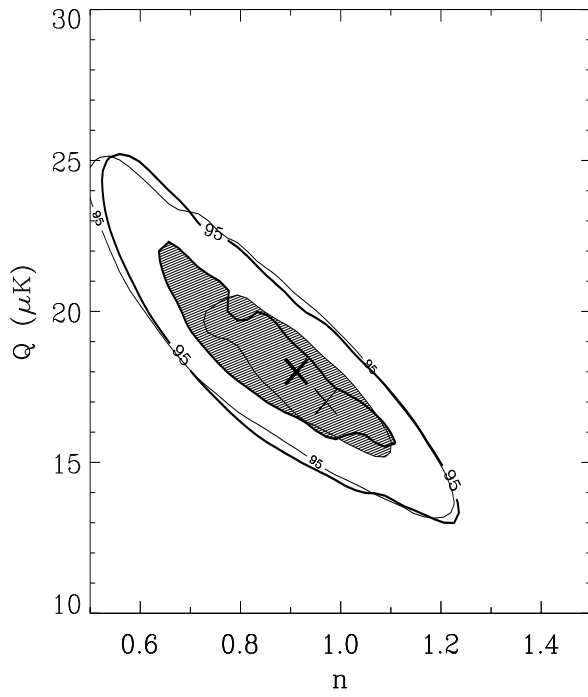


**Fig. 17.** Likelihood contours in the  $n - Q$  plane for  $h$  free and  $\Omega_b$  free. The region  $n \lesssim 0.8$ ,  $Q \gtrsim 20 \mu\text{K}$  (which has  $h \sim 1.00$ ) is not disjoint from the low  $h$  region.